Bioconjugate Chemistry

Article

pubs.acs.org/bc

Functionalized Low-Density Lipoprotein Nanoparticles for in Vivo Enhancement of Atherosclerosis on Magnetic Resonance Images

Andrew N. Lowell,[†] Hui Qiao,[§] Ting Liu,[§] Takashi Ishikawa,[‡] Hualei Zhang,[§] Sean Oriana,[#] Miao Wang,[∥,⊥] Emanuela Ricciotti,[∥,⊥] Garret A. FitzGerald,[∥,⊥] Rong Zhou,[*,⊥,§] and Yoko Yamakoshi[*,§,#]

[†]Department of Chemistry, and [§]Molecular Imaging Laboratories, Department of Radiology, University of Pennsylvania, 231 South 34th Street, Philadelphia, Pennsylvania 19104-6323, United States

[‡]Paul-Scherrer Institute, CH-5232, Villigen, Switzerland

[∥]Department of Pharmacology and [⊥]Institute for Translational Medicine and Therapeutics (ITMAT), University of Pennsylvania, 3400 Civic Center Boulevard, Philadelphia, Pennsylvania 19104-6160, United States

[#]Laboratorium für Organische Chemie, ETH-Zürich, Wolfgang-Pauli-Strasse 10, CH-8093 Zürich, Switzerland

Supporting Information

ABSTRACT: To allow visualization of macrophage-rich and miniature-sized atheromas by magnetic resonance (MR) imaging, we have converted low-density lipoprotein (LDL) into MR-active nanoparticles via the intercalation of a 1,4,7,10-tetraazacyclodecane-1,4,7-triacetic acid (DO3A) derivative and the subsequent coordination reaction with Gd^{3+}. After careful removal of nonchelated Gd^{3+}, an MR-active LDL (Gd^{3+}-LDL) with a remarkably high payload of Gd^{3+} (in excess of 200 Gd^{3+} atoms per particle) and a high relaxivity (r_1 = 20.1 s^{-1} mM^{-1} per Gd^{3+} or 4040 s^{-1} mM^{-1} per LDL) was obtained. Dynamic light-scattering photon correlation spectroscopy (DLS) and cryo transmission electron microscope (cryoTEM) images showed that Gd^{3+}-LDL particles did not aggregate and remained of a similar size (25−30 nm) to native LDL. Intravenous injection of Gd^{3+}-LDL into an atherosclerotic mouse model (*ApoE*$^{-/-}$) resulted in an extremely high enhancement of the atheroma-bearing aortic walls at 48 h after injection. Free Gd^{3+} dissociation from Gd^{3+}-LDL was not detected over the imaging time window (96 h). Because autologous LDL can be isolated, modified, and returned to the same patient, our results suggest that MR-active LDL can potentially be used as a noninfectious and nonimmunogenic imaging probe for the enhancement of atheroplaques presumably via the uptake into macrophages inside the plaque.

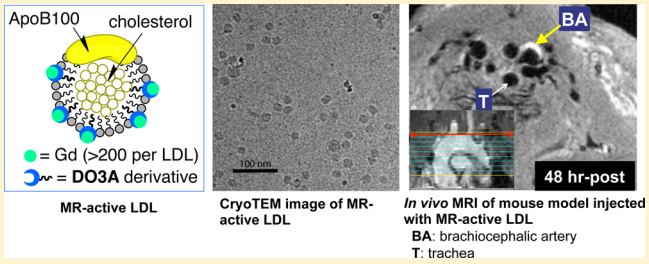

INTRODUCTION

The blockage of coronary and carotid arteries due to the growth or rupture of atherosclerotic plaques (atheromas) often leads to lethal syndromes such as heart attack and stroke, which are the leading causes of death worldwide. Magnetic resonance imaging (MRI), owing to its high soft tissue contrast and high spatial resolution, is well suited for visualizing atheroplaques harbored in the aortic wall in a noninvasive manner. While MR imaging of atheromas enriched with macrophages or other inflammatory effector cells has been attempted using contrast agents (CAs) with various nanoparticle scaffolds such as polymeric materials,[1−4] micelles or liposomes,[5−8] and high-density lipoprotein (HDL),[6,9−19] the potential of modifying naturally occurring low-density lipoprotein (LDL) nanoparticles for MR imaging of atheromas has not been assessed so far. The critical role of LDL in the formation and progression of atherosclerosis has been well established by epidemiological studies, which revealed a high correlation between the plasma LDL level and the chance of the patient to develop atherosclerosis or to die from coronary heart disease. In addition, the idea of infusing the patient's own LDL labeled with an MR-active probe, converting it into a nonimmunogenic targeting vehicle to visualize inflammatory atheroplaques, is a powerful example of personalized medicine.

The present study describes the resolution of a number of challenges that allowed us to realize a strong and discrete enhancement of submillimeter-size mouse atheromas on MR images. Most importantly, a high payload of MR contrast molecules (Gd^{3+}-chelate) per LDL particle was achieved. Toxic unbound Gd^{3+} were successfully eliminated to provide a good safety profile for these nanoparticles, and the modified LDL remained stable during the imaging time window (at least 96 h) without detectable dissociation of Gd^{3+} and maintained a size distribution similar to that of native LDL.

EXPERIMENTAL PROCEDURES

Synthesis of a DO3A Derivative for Intercalation into LDL.[20] DO3A−oleic acid conjugate **A** (1,4,7,10-tetraazacyclodecane-1,4,7-triacetic acid-oleic acid, DO3A-OA) was synthe-

Received: October 12, 2012
Published: October 18, 2012

sized as shown in Scheme 1 by the conjugation of oleic acid to *t*-butyl protected DO3A (**2**) via a diamine. Purification of the products and intermediates was carried out by HPLC (JASCO PU-2080 pump and UV-2077 plus UV–vis detector, JASCO Co., Tokyo, Japan) with a reversed-phase semipreparatory column (YMC R-ODS-10A 250 × 20 mm, YMC Co., Ltd., Kyoto, Japan). As **A** was not visible by UV–vis detection, all the fractions were collected from the semipreparative HPLC and analyzed by both an analytical HPLC (YMC R-ODS-10A 250 × 4.6 mm) equipped with a Nano Quantity Analyte Detector (NQAD, Quant Technology, Blaine, MN, USA) and ESI-MS (Waters SQD and Acuity UPLC, Waters Co., Milford, MA, USA). After purification, the purity of **A** was checked again by HPLC with a reversed-phase analytical column (YMC R-ODS-10A, 250 × 4.6 mm) and then was fully characterized by ^{1}H and ^{13}C NMR (Bruker Advance AVII-500 NMR spectrometer, Bruker, Billerica, MA, USA), HR-MS (Waters LCT Premier XE LC/MS system), and FT-IR (JASCO FT/IR-4100).

Scheme 1. Synthesis of DO3A-OA (A)

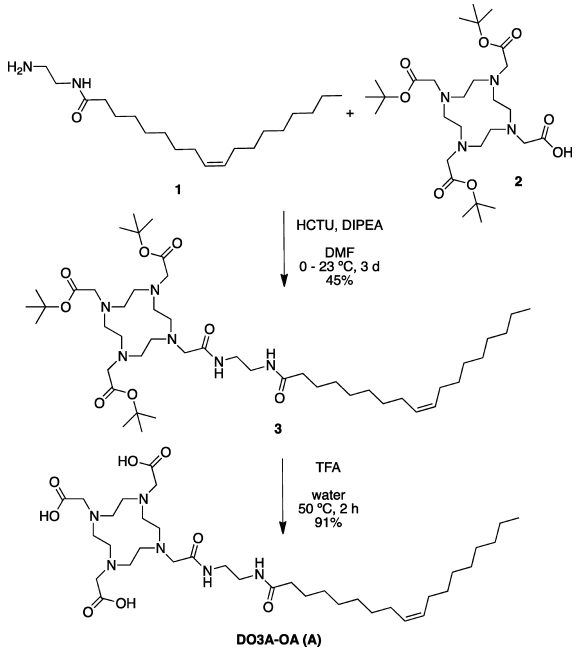

LDL. Human LDL (density 1.024–1.050 g/mL) was isolated from the fresh plasma of healthy normolipidemic donors by sequential density gradient ultracentrifugation in the laboratory of Dr. Lund-Katz at the Children's Hospital of Philadelphia[21] and was filtered (0.22 μm Millex GVdurapore PVDF membrane filter, Millipore, Billerica, MA, USA) and dialyzed (Spectra/Por4 dialysis tubing with a flat width of 25 mm and a MWCO of 12–14 kD, Spectrum Laboratories, Inc., Rancho Dominguez, CA, USA) against phosphate buffered saline, Ca^{2+} and Mg^{2+} free, (PBS(−)) at 4 °C for 20 h before use. The amount of LDL was estimated from its protein content as calculated by the Lowry assay (Peterson's modification, Sigma-Aldrich, St. Louis, MO, USA)[22,23] based on the assumption that only one copy of apoB-100 protein (MW 534 kD) presents per LDL nanoparticle.[24]

General Preparation of Gd^{3+}-LDL.[25] Compound **A** was dissolved in a minimal amount of DMSO (~0.1 mL). Dialyzed LDL was added to this solution in a molar ratio of approximately 1:600 (LDL:**A**). The mixture was agitated at 37 °C for 4 h on a circular shaker (120 rpm), filtered (0.22 μm Millex), and dialyzed (Spectra/Por4) against PBS(−) at 4 °C for 16 h to remove unbound **A** (*STEP 1* in Figure 2). Gd^{3+} citrate solution (2.1 mM) was added to the LDL sample in a molar ratio of approximately 1400:1 Gd^{3+} to LDL and the mixture was agitated (120 rpm) at 37 °C for 4 h (*STEP 2* in Figure 2). Freshly prepared tropolone solution in PBS(−) (10 mM) was added in excess to the Gd^{3+}-treated LDL sample (*STEP 3* in Figure 2, 15 mol equiv of tropolone was used for each equivalent of Gd^{3+} used during *STEP 2*),[26,27] and the resulting mixture was agitated (4 °C, 120 rpm, 4 h). The precipitated Gd^{3+}-tropolone complex was removed by filtration (0.22 μm), and the filtrate was subsequently dialyzed against PBS(−) (4 °C, 120 rpm, 18 h).

DLS. The particle size of intact LDL or modified LDL was analyzed by dynamic light-scattering photon correlation spectroscopy (DLS, Zetasizer 3000HS, Malvern Instruments, Malvern, UK) on a spectrometer equipped with a 10 mW He–Ne laser operating at a fixed wavelength of 633 nm and a detector angle of 90°. The data, in the form of autocorrelation functions, were analyzed assuming that the particles were spherical and undergoing Brownian motion.

ICP-MS. The ICP-MS analysis of the Gd^{3+} content of functionalized LDL (ng of Gd^{3+} per mg of LDL sample) was carried out at the Pennsylvania Animal Diagnostic Laboratory System in New Bolton Center (Kennett Square, PA, USA).

CryoTEM.[28] An aliquot (3.5 μL) of the LDL or modified LDL specimen was mounted on holey carbon grids (Quantifoil Micro Tools GmbH, Jena, Germany) and frozen using a Vitrobot apparatus (FEI Co., Eindhoven, Netherlands). The grids were examined at liquid nitrogen temperature using a cryo-holder (626, Gatan, Inc., Pleasanton, CA, USA) and a Tecnai G2 F20 microscope (FEI Co.) equipped with a field emission gun and an energy filter (Tridem, Gatan, Inc.) operated at an accelerating voltage of 200 kV. The data were recorded by a 2k × 2k CCD camera (US1000, Gatan, Inc.) with an underfocus of 4–7 μm. Each image was recorded with a dose of ~10 $e^{-}/Å^{2}$.

Relaxivity. The proton longitudinal relaxation rates ($1/T_1$) were measured on an mq60 minispec NMR Analyzer (Bruker, Inc., The Woodlands, TX, USA) at 60 MHz. The T_1 measurements were carried out in PBS(−) with an inversion–recovery pulse sequence using 10 to 20 inversion delay values. The r_1 relaxivity was calculated from the slope of a plot of $1/T_1$ versus Gd^{3+} concentration.

Animal Models. *ApoE*$^{-/-}$ mice and their wild-type controls (C57BL/6j) were purchased from Jackson Laboratory (Bar Harbor, ME, USA). The *ApoE*$^{-/-}$mice were fed a high fat diet (0.2% cholesterol, 21% saturated fat; formula TD 88137, Harlan Laboratories, Indianapolis, IN, USA) for 4–5 months to expedite the development of atheromas, while the C57BL/6j mice were on normal chow.

In Vivo MR Imaging. All the procedures were carried out in accordance with the in vivo animal protocols approved by the Institutional Animal Care and Use Committee at the University of Pennsylvania. Prior to the injection, the Gd^{3+}-LDL sample was concentrated in filter tubes (Amcon Ultra-4) by centrifugation (3000 rpm at 4 °C) to a suitable volume (≤0.5 mL) for tail vein injection into a mouse. No aggregation was detected after the centrifugation. Animals were positioned prone in a quadrature volume ^{1}H coil (i.d. = 3.5 cm, length = 8 cm), which was interfaced to a 9.4 T horizontal bore MR

spectrometer (DirectDrive, Varian, Palo Alto, CA). During imaging, the animal was sedated with 0.8−1% of isoflurane, and its vital signs (including ECG, respiration, and core temperature) were monitored. The rectal temperature was maintained at 36 °C by directing warm air into the magnet bore. "White Blood" (WB) images, where the blood signal in the aorta lumen is not suppressed, were acquired using a multislice gradient echo sequence (TR = 1 heart beat, about 120 ms, TE = 2.4 ms), while "Black Blood" (BB) images, where the blood signal is suppressed, were obtained using a multislice fast spin echo sequence (TR = 1000 ms, TE =10.4 ms, echo train length =1). For both WB and BB images, field of view (FOV) = 26 × 26 mm^2, matrix size = 256 × 192, and slice thickness = 0.5 mm. The percent of normalized signal enhancement, %NSE,[29,30] was measured for enhanced versus unenhanced artery walls on MR images.

RESULTS AND DISCUSSION

Synthesis of DO3A-OA (A) and Modification of LDL. To achieve a high payload of Gd^{3+}, we implemented a method where DO3A-OA (**A** in Scheme 1) was first intercalated into the lipid monolayer of LDL and then subjected to a coordination reaction with Gd^{3+}. This approach allowed higher yields in the initial intercalation step by taking advantage of the higher water-solubility of **A** as opposed to prechelated Gd**A**, which is poorly soluble, to provide LDL nanoparticles with a remarkably high Gd^{3+} payload. The synthesis of **A** is described in the Methods section and is shown in Scheme 1.[31] The DO3A moiety was chosen as the ligand due to its higher affinity for Gd^{3+} compared to other common Gd^{3+}-ligands such as diethylenetriaminepentaacetic acid (DTPA, Figure 1) while providing the same level of contrast enhancement.[32,33]

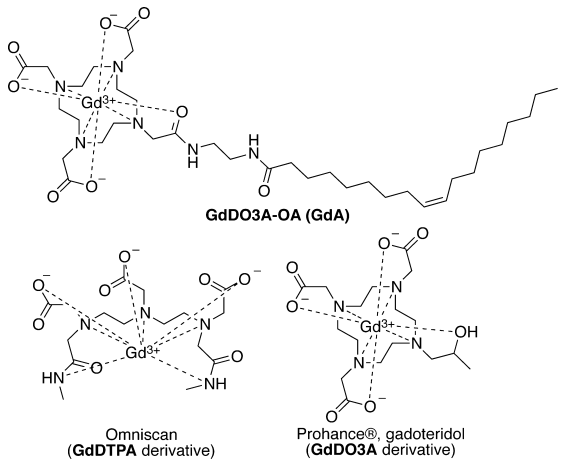

Figure 1. Structures of **GdDO3A-OA** (**GdA**) designed for LDL modification in this study and MRI contrast agents (Omniscan and Prohance) approved by the FDA for routine clinical use.

The general scheme for infusing LDL nanoparticles with Gd^{3+} and the optimizations used to achieve a high loading are shown in Table 1. After the intercalation of **A** into LDL (*STEP 1*), the Gd^{3+} coordination was carried out by exposing the LDL-**A** particles to Gd^{3+} citrate (*STEP 2*).

Because a substantial amount of the potentially toxic Gd^{3+} was expected to bind nonspecifically on the surface of LDL without chelating to the DO3A moiety, its efficient removal was investigated in detail (*STEP 3* of Table 1). For the removal of such nonspecifically bound Gd^{3+}, a tropolone precipitation protocol was used (scheme in a footnote of Table 1). Tropolone is known to strongly coordinate Gd^{3+} resulting in an insoluble precipitate that can be removed by filtration.[27,34] As a control, intact LDL without **A** was subjected to the same Gd^{3+} chelation conditions with Gd^{3+} citrate as were used for LDL-**A** (*STEP 2*) and subsequently treated with tropolone (*STEP 3*). Initial reaction conditions with a short incubation interval (1 h) and a diluted condition in *STEP 2* did not remove the nonspecifically bound Gd^{3+} from the surface of LDL efficiently (68 atoms of Gd^{3+} per LDL were still remaining, Table 1 run 1). By extending the reaction time (4 h) and reducing the reaction volume (1.5 mL), efficient removal could be achieved (only 2 atoms of Gd^{3+} per LDL remained, Table 1 run 3). Application of these optimized conditions to LDL-**A** resulted in a significantly higher Gd^{3+} loading (20 atoms per LDL, Table 1 run 4) showing that Gd^{3+} specifically bound to the DO3A moiety was retained by the LDL.

Further efforts to increase the payload of Gd^{3+} per LDL were carried out by increasing equivalents of **A** and Gd^{3+} citrate in *STEPs 1* and *2*, respectively, and provided a significantly higher loading rate (210 Gd^{3+} per LDL, Table 1 run 5). A control reaction with intact LDL confirmed that the tropolone treatment remained effective at these higher Gd^{3+} condition (2 Gd^{3+} per LDL, run 6). This high payload of Gd^{3+} per LDL is a 40-fold increase compared to our preliminary study where one-step modification of LDL with premade Gd**A** led to only 5 Gd^{3+} per LDL due to the lower solubility of Gd**A**.[29]

Characterization of Gd^{3+}-LDL by DLS, CryoTEM, and Relaxivity Measurements. Because the aggregation of particles affects their availability to target tissues, LDL particle morphology before and after modification was carefully examined. Dynamic light-scattering photon correlation spectroscopy (DLS) and single particle observation using a cryo transmission electron microscope (cryoTEM) were used to analyze the particle diameter distribution. DLS showed that, when compared to intact LDL (mean 25 nm, width 13 nm, Figure 2c), Gd^{3+}-LDL remained in the similar size (mean 28 nm, width 16 nm, Figure 2a) and did not significantly aggregate through the modification. This result was consistent with cryoTEM images of Gd^{3+}-LDL and intact LDL (Figure 2b,d) and suggested that Gd^{3+}-LDL could be used for tail vein injection in mice without causing adverse effects.

The proton longitudinal relaxation rate ($1/T_1$) of Gd^{3+}-LDL nanoparticle was measured at 60 MHz (Table 2). The r_1 relaxivity of Gd^{3+}-LDL (200 Gd^{3+} per particle) was 20.2 s^{-1} mM^{-1} per Gd^{3+} (4040 s^{-1} mM^{-1} per particle), which is much higher than small molecule contrast agent Prohance (3.77 s^{-1} mM^{-1} per Gd^{3+} at 60 MHz[35]). Gd^{3+}-LDL with lower loadings (40 Gd^{3+} per particle) gave a relaxivity per Gd^{3+} of 12.1 s^{-1} mM^{-1}. The higher relaxivity of Gd^{3+}-LDL with 200 Gd^{3+} per particle could result from a slower tumbling rate of the labeled LDL.

Stability of Gd^{3+}-LDL Particles. The stability of the LDL nanoparticles was analyzed by observing changes in particle morphology and the dissociation of free Gd^{3+} by DLS and ICP-MS measurements, respectively. The Gd^{3+}-LDL nanoparticles were kept at 4 or −20 °C in PBS(−) for a variable time period and then analyzed by DLS. The particle size remained regular for approximately 6 days at 4 °C. After 10−18 days of storage at 4 °C, however, the particle size gradually increased from the intact size of 20−30 nm to >40 nm (mean) with the appearance of a small, broad distribution around 150−200

Table 1. Reaction Conditions for the Preparation of MR-Active LDL Nanoparticles by the Intercalation of A (*STEP 1*), Chelation with Gd^{3+} (*STEP 2*), and Removal of Uncoordinated Gd^{3+} with Tropolone (*STEP3*)

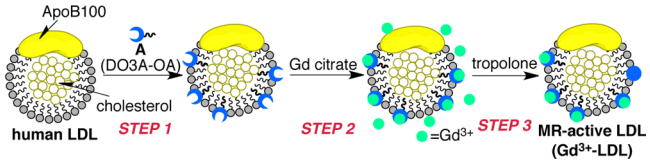

	STEP 1		*STEP 2*	*STEP 3*[b]			
				reaction conditions with tropolone			
run	initial amount of LDL [mmol][a]	mol. ratio of **A** [eq. to LDL]	mol. ratio of Gd^{3+} [eq. to LDL]	time [h]	rection volume [mL]	Gd^{3+} atoms per LDL particle[c]	DLS mean (SE) [nm]
1	2.25×10^{-6}	0	156	1	4.5	68	31.3 (25.5)
2	2.12×10^{-6}	0	189	4	5.0	20	24.9 (13.2)
3	2.12×10^{-6}	0	189	4	1.5	2	20.9 (17.5)
4	2.12×10^{-6}	123	189	4	1.5	20	28.0 (15.8)
5	7.42×10^{-5}	665	1401	4	60	210	26.3 (16.3)
6	1.48×10^{-6}	0	1401	4	1.2	2	23.8 (12.2)

[a]Estimated by Lowry test. [b]The 15 mol equivalents of tropolone were added to each Gd^{3+} used in *STEP2*. Reaction was carried out at 4 °C. Reaction scheme of Gd^{3+} and tropolone:

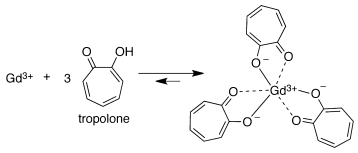

[c]Obtained by ICP-MS analysis.

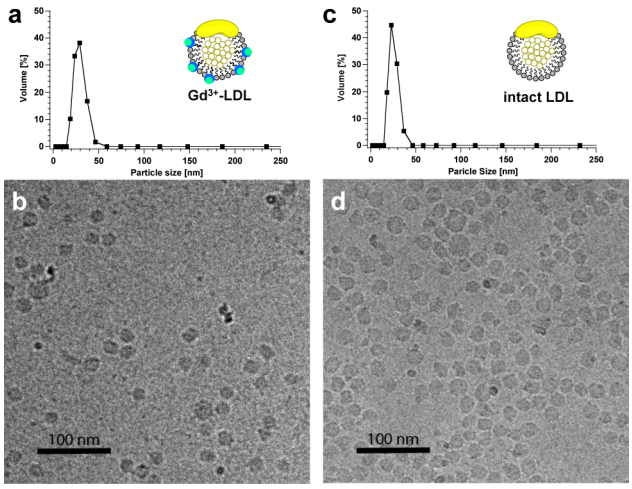

Figure 2. DLS and cryoTEM images of Gd^{3+}-LDL (a and b) and intact LDL (c and d) nanoparticles. Both data sets indicate that both the modified and intact LDL nanoparticles exist as dispersed single particles in buffer (the small dark spots in cryoTEM images are ice crystals generated during sample preparation).

nm to indicate that aggregation was starting (Figure S3 in the SI). The frozen samples, however, did not show significant aggregation after 34 days stored at −20 °C (Figure S3f in the SI).

A Gd^{3+} leaching experiment was carried out over the same time window (96 h) within which the MR imaging was performed by dialyzing an aliquot of Gd^{3+}-LDL against PBS(−) at 4 °C. Quantification by ICP-MS of the amount of Gd^{3+} in the sample inside the dialysis tube showed no significant change over 96 h (Table S5 in the SI). The Gd^{3+} level of the sample outside the dialysis tube at 96 h was below ICP-MS detection limit, also indicating that no Gd^{3+} dissociated from the particles over the 96 h period.

Table 2. Comparison of the Relaxivity of Gd^{3+}-LDL and Gadoteridol[a]

contrast agents	r_1 relaxivity per Gd^{3+} [mM^{-1} s^{-1}]	r_1 relaxivity per particle [mM^{-1} s^{-1}]
Gd^{3+}-LDL (40:1)	12.1	484
Gd^{3+}-LDL (200:1)	20.2	4040
Gadoteridol (Prohance)	3.8	–

[a]Relaxivity measurements were carried out at 60 MHz and at room temperature. The numbers 40:1 and 200:1 indicate the molar ratios of Gd^{3+} to LDL, which were calculated from the results of ICP-MS analysis and the Lowry assay, respectively.

In Vivo MRI of Atheroma in Mice Receiving Gd^{3+}-LDL. In order to assess the utility of Gd^{3+}-LDL for the enhancement of atheromas, in vivo studies were carried out in a murine atherosclerosis model and its control. *ApoE*$^{-/-}$ mice and their wild-type controls (C57BL/6j) weighing 20−42 g were injected with Gd^{3+}-LDL at Gd^{3+} doses of 0.019−0.055 mmol/kg via the tail vein. A serial in vivo MRI was performed on *ApoE*$^{-/-}$ and C57BL/6j mice pre- and 24−96 h post-Gd^{3+}-LDL injection. Because the animals were allowed to recover from anesthesia during the interval of the pre- and postinjection imaging sessions, we relied on the unique anatomy of the thoracic arteries for the comparison of pre- and postinjection images. Specifically, the thoracic aorta, including the aortic arch and its three branches, was visualized on coronal scout images as shown in the inset of Figure 3a−c. The orientation of these vessels was matched on the pre- and postinjection images to ensure that the identical plaque region was compared. On the basis of the scout images, multiple axial images were acquired in

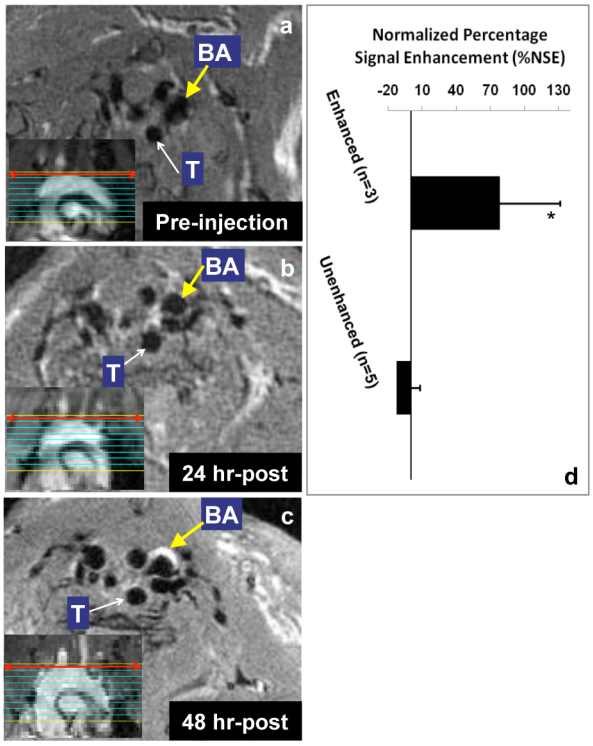

Figure 3. (a–c) In vivo MR images of an atheroma in the artery of an *ApoE*$^{-/-}$ mouse taken preinjection (a) and 24 h (b) and 48 h after injection (c) of Gd^{3+}-LDL (T = trachea, BA = brachiocephalic artery). The inset images in a–c are scout images in the coronal view where the thoracic aorta and its three branches are clearly shown; the branch on the left is the BA. The red line in the scout images indicates the position of the axial image shown in the same panel. (d) Signal enhancement estimated from MR images by the formula below using the chest muscle as a reference (p = 0.01 comparing enhanced versus unenhanced arteries by the Student's t-test). %NSE =100% × $((I_{wallpost}/I_{musclepost})/(I_{wallpre}/I_{musclepre}) - 1)$. $I_{wallpre}$ and $I_{wallpost}$ are signal intensity from the artery wall pre- and 48 h postinjection, respectively. $I_{musclepre}$ and $I_{musclepost}$ are defined similarly.

"white blood" (WB) or "black blood" (BB) fashion. BB images, in which the blood signals were suppressed, can better visualize the artery wall. As shown in Figure 3a–c, a remarkably intense enhancement of the wall of the brachiocephalic artery (BA) was detected at 48 h postinjection, whereas images obtained at 24 h show little enhancement compared to the preinjection image (the entire data sets of preinjection, 24 h and 48 h postinjectin for the mouse shown in Figure 3 are provided in Figure S6 in the SI). Despite the limited volume of Gd^{3+}-LDL that can be administrated intravenously to a mouse (≤0.5 mL), the strong enhancement of miniature-sized murine atheromas was observed suggesting that the payload of Gd^{3+} and selective LDL accumulation into atheroma were sufficient for the enhancement. The normalized signal enhancement (%NSE is defined in the caption of Figure 3) suggests an excellent contrast between the enhanced and unenhanced artery walls on MR images of *ApoE*$^{-/-}$ mice. No significant enhancement was found on images obtained from control (C57BL/6j) mice (data not shown).

■ CONCLUSION

While LDL has been utilized as a cancer-targeting vehicle for the efficient delivery of anticancer drugs[36−38] and imaging probes[27,34,39−48] based on the overexpression of LDL receptors on many malignant cancers, the utility of this natural nanoparticle has not been reported for MR imaging of atheroplaques, especially those that are prone to rupture due to a high content of inflammatory cells such as macrophages. The MR-active LDL reported here carries a high payload of Gd^{3+} (>200 Gd^{3+} atoms per particle). The high relaxivity of the nanoparticle led to discrete enhancement of an aortic wall bearing atheroplaques on MR images. The efficient loading of Gd^{3+} has the following important consequences: (1) the dose of LDL that needs to be administered into animals (or patients) can be reduced while providing sufficient MRI enhancement; (2) highly efficient enhancement, which is necessary for visualizing lesions inside of the aorta wall, can be attained as demonstrated in the images of a minuscule murine atheroma. The LDL nanoparticles circulating in the blood of hyperlipidemia patients directly participates in the growth of atheroplaques because they are absorbed by macrophages residing in the plaque. Therefore, macrophages could be the specific cellular component of the atheroplaque that absorbs the Gd^{3+}-LDL nanoparticles, but further validation is needed. While the long-term safety of Gd^{3+}-LDL still needs to be demonstrated, we have shown that the particles did not aggregate and remained in the 20−30 nm size range. Importantly, leaching of toxic free Gd^{3+} from the particles was not detectable by ICP-MS. We conclude that human LDL can be converted into nontoxic, nonimmunogenic, and highly MR-active nanoparticles for the selective detection of atherosclerotic plaques by high-resolution MRI. This work lays the foundation for exploring a personalized medicine strategy by directing a patient's own LDL to the inflammatory effector cells in vulnerable atheroplaques.

■ ASSOCIATED CONTENT

Ⓢ Supporting Information

Details of the synthesis of probe **A**, particle preparation, and in vivo experiments. This material is available free of charge via the Internet at http://pubs.acs.org.

■ AUTHOR INFORMATION

Corresponding Author

*E-mail: yamakoshi@org.chem.ethz.ch; zhou@rad.upenn.edu.

Notes

The authors declare no competing financial interest.

■ ACKNOWLEDGMENTS

The authors thank Prof. Dr. Daniel Rader and Prof. Dr. Sissel Lund-Katz for their insightful discussions on modifying human LDL for imaging atherosclerosis, Dr. Hoon Choi and Prof. Dr. I-Wei Chen for their help with the dynamic light scattering measurements, Prof. Dr. Andrew Tsourkas for his assistance with the relaxation time measurements, and Prof. Dr. Jerry Glickson and Dr. Hui Li for their helpful discussions at the University of Pennsylvania. This study was supported in part by a Scientist Development Awards from the American Heart Association (No. 0930140N (Y.Y.)), the PRESTO program of the Japan Science and Technology Agency (Y.Y.), in part by Grant Number UL1RR024134 from the National Center for Research Resources of NIH, and in part by the Institute for Translational Medicine and Therapeutics (ITMAT) Transdisciplinary Program in Translational Medicine and Therapeutics of the University of Pennsylvania (R.Z.). The use of electron microscopy in EMEZ (EM Center) in ETH Zürich

and MRI in SAIF (Small Animal Imaging Facility) at the University of Pennsylvania are also acknowledged.

REFERENCES

(1) Aime, S., Botta, M., Geninatti Crich, S., Giovenzana, G., Palmisano, G., and Sisti, M. (1999) Novel paramagnetic macromolecular complexes derived from the linkage of a macrocyclic Gd(III) complex to polyamino acids through a squaric acid moiety. *Bioconjugate Chem. 10*, 192−199.

(2) Park, K., Hong, H. Y., Moon, H. J., Lee, B. H., Kim, I. S., Kwon, I. C., and Rhee, K. (2008) A new atherosclerotic lesion probe based on hydrophobically modified chitosan nanoparticles functionalized by the atherosclerotic plaque targeted peptides. *J. Controlled Release 128*, 217−223.

(3) Nahrendorf, M., Keliher, E., Marinelli, B., Waterman, P., Feruglio, P. F., Fexon, L., Pivovarov, M., Swirski, F. K., Pittet, M. J., Vinegoni, C., and Weissleder, R. (2010) Hybrid PET-optical imaging using targeted probes. *Proc. Natl. Acad. Sci. U. S. A. 107*, 7910−7915.

(4) Chan, J. M., Zhang, L., Tong, R., Ghosh, D., Gao, W., Liao, G., Yuet, K. P., Gray, D., Rhee, J. W., Cheng, J., Golomb, G., Libby, P., Langer, R., and Farokhzad, O. C. (2010) Spatiotemporal controlled delivery of nanoparticles to injured vasculature. *Proc. Natl. Acad. Sci. U. S. A. 107*, 2213−2218.

(5) Peters, D., Kastantin, M., Kotamraju, V. R., Karmali, P. P., Gujraty, K., Tirrell, M., and Ruoslahti, E. (2009) Targeting atherosclerosis by using modular, multifunctional micelles. *Proc. Natl. Acad. Sci. U. S. A. 106*, 9815−9819.

(6) Beilvert, A., Cormode, D. P., Chaubet, F., Briley-Saebo, K. C., Mani, V., Mulder, W. J., Vucic, E., Toussaint, J. F., Letourneur, D., and Fayad, Z. A. (2009) Tyrosine polyethylene glycol (PEG)-micelle magnetic resonance contrast agent for the detection of lipid rich areas in atherosclerotic plaque. *Magn. Reson. Med. 62*, 1195−1201.

(7) Srinivasan, R., Marchant, R. E., and Gupta, A. S. (2010) In vitro and in vivo platelet targeting by cyclic RGD-modified liposomes. *J. Biomed. Mater. Res. A 93*, 1004−1015.

(8) van Tilborg, G. A., Vucic, E., Strijkers, G. J., Cormode, D. P., Mani, V., Skajaa, T., Reutelingsperger, C. P., Fayad, Z. A., Mulder, W. J., and Nicolay, K. (2010) Annexin A5-functionalized bimodal nanoparticles for MRI and fluorescence imaging of atherosclerotic plaques. *Bioconjugate Chem. 21*, 1794−1803.

(9) Briley-Saebo, K. C., Mulder, W. J., Mani, V., Hyafil, F., Amirbekian, V., Aguinaldo, J. G., Fisher, E. A., and Fayad, Z. A. (2007) Magnetic resonance imaging of vulnerable atherosclerotic plaques: current imaging strategies and molecular imaging probes. *J. Magn. Reson. Imaging 26*, 460−479.

(10) Sanz, J., and Fayad, Z. A. (2008) Imaging of atherosclerotic cardiovascular disease. *Nature 451*, 953−957.

(11) Douma, K., Prinzen, L., Slaaf, D. W., Reutelingsperger, C. P., Biessen, E. A., Hackeng, T. M., Post, M. J., and van Zandvoort, M. A. (2009) Nanoparticles for optical molecular imaging of atherosclerosis. *Small 5*, 544−557.

(12) Buxton, D. B. (2009) Current status of nanotechnology approaches for cardiovascular disease: a personal perspective. *Wiley Interdiscip. Rev. Nanomed. Nanobiotechnol. 1*, 149−155.

(13) Frias, J. C., Williams, K. J., Fisher, E. A., and Fayad, Z. A. (2004) Recombinant HDL-like nanoparticles: a specific contrast agent for MRI of atherosclerotic plaques. *J. Am. Chem. Soc. 126*, 16316−16317.

(14) Cormode, D. P., Briley-Saebo, K. C., Mulder, W. J., Aguinaldo, J. G., Barazza, A., Ma, Y., Fisher, E. A., and Fayad, Z. A. (2008) An ApoA-I mimetic peptide high-density-lipoprotein-based MRI contrast agent for atherosclerotic plaque composition detection. *Small 4*, 1437−1444.

(15) Chen, W., Vucic, E., Leupold, E., Mulder, W. J., Cormode, D. P., Briley-Saebo, K. C., Barazza, A., Fisher, E. A., Dathe, M., and Fayad, Z. A. (2008) Incorporation of an apoE-derived lipopeptide in high-density lipoprotein MRI contrast agents for enhanced imaging of macrophages in atherosclerosis. *Contrast Media Mol. Imaging 3*, 233−242.

(16) Cormode, D. P., Chandrasekar, R., Delshad, A., Briley-Saebo, K. C., Calcagno, C., Barazza, A., Mulder, W. J., Fisher, E. A., and Fayad, Z. A. (2009) Comparison of synthetic high density lipoprotein (HDL) contrast agents for MR imaging of atherosclerosis. *Bioconjugate Chem. 20*, 937−943.

(17) Skajaa, T., Zhao, Y., van den Heuvel, D. J., Gerritsen, H. C., Cormode, D. P., Koole, R., van Schooneveld, M. M., Post, J. A., Fisher, E. A., Fayad, Z. A., de Mello Donega, C., Meijerink, A., and Mulder, W. J. (2010) Quantum dot and Cy5.5 labeled nanoparticles to investigate lipoprotein biointeractions via Forster resonance energy transfer. *Nano Lett. 10*, 5131−5138.

(18) Thaxton, C. S., Daniel, W. L., Giljohann, D. A., Thomas, A. D., and Mirkin, C. A. (2009) Templated spherical high density lipoprotein nanoparticles. *J. Am. Chem. Soc. 131*, 1384−1385.

(19) Mackiewicz, M. R., Hodges, H. L., and Reed, S. M. (2010) C-reactive protein induced rearrangement of phosphatidylcholine on nanoparticle mimics of lipoprotein particles. *J. Phys. Chem. B 114*, 5556−5562.

(20) The detail of the synthesis and spectroscopic data are provided in the SI.

(21) Lund-Katz, S., Laplaud, P. M., Phillips, M. C., and Chapman, M. J. (1998) Apolipoprotein B-100 conformation and particle surface charge in human LDL subspecies: implication for LDL receptor interaction. *Biochemistry 37*, 12867−12874.

(22) Lowry, O. H., Rosebrough, N. J., Farr, A. L., and Randall, R. J. (1951) Protein measurement with the Folin phenol reagent. *J. Biol. Chem. 193*, 265−275.

(23) Peterson, G. L. (1977) A simplification of the protein assay method of Lowry et al. which is more generally applicable. *Anal. Biochem. 83*, 346−356.

(24) Protein content values were 1.9−3.8 mg/mL.

(25) Details are described in the SI.

(26) Tropolone concentration for removal of Gd3+ from the nanoparticle solution was optimized as shown in Table S3 of SI.

(27) Jasanada, F., Urizzi, P., Souchard, J. P., Le Gaillard, F., Favre, G., and Nepveu, F. (1996) Indium-111 labeling of low density lipoproteins with the DTPA-bis(stearylamide): evaluation as a potential radiopharmaceutical for tumor localization. *Bioconjugate Chem. 7*, 72−81.

(28) Ishikawa, T., Sakakibara, H., and Oiwa, K. (2007) The architecture of outer dynein arms in situ. *J. Mol. Biol. 368*, 1249−1258.

(29) Yamakoshi, Y., Qiao, H., Lowell, A. N., Woods, M., Paulose, B., Nakao, Y., Zhang, H. L., Liu, T., Lund-Katz, S., and Zhou, R. (2011) LDL-based nanoparticles for contrast enhanced MRI of atheroplaques in mouse models. *Chem. Commun. 47*, 8835−8837.

(30) van Bochove, G. S., Paulis, L. E. M., Segers, D., Mulder, W. J. M., Krams, R., Nicolay, K., and Strijkers, G. J. (2011) Contrast enhancement by differently sized paramagnetic MRI contrast agents in mice with two phenotypes of atherosclerotic plaque. *Contrast Media Mol. Imaging 6*, 35−45.

(31) The detailed synthetic procedure is described in SI.

(32) Magerstadt, M., Gansow, O. A., Brechbiel, M. W., Colcher, D., Baltzer, L., Knop, R. H., Girton, M. E., and Naegele, M. (1986) Gd(DOTA): an alternative to Gd(DTPA) as a T1,2 relaxation agent for NMR imaging or spectroscopy. *Magn. Reson. Med. 3*, 808−812.

(33) Nwe, K., Bernardo, M., Regino, C. A., Williams, M., and Brechbiel, M. W. (2010) Comparison of MRI properties between derivatized DTPA and DOTA gadolinium-dendrimer conjugates. *Bioorg. Med. Chem. 18*, 5925−5931.

(34) Corbin, I. R., Li, H., Chen, J., Lund-Katz, S., Zhou, R., Glickson, J. D., and Zheng, G. (2006) Low-density lipoprotein nanoparticles as magnetic resonance imaging contrast agents. *Neoplasia 8*, 488−498.

(35) Mastarone, D. J., Harrison, V. S., Eckermann, A. L., Parigi, G., Luchinat, C., and Meade, T. J. (2011) A modular system for the synthesis of multiplexed magnetic resonance probes. *J. Am. Chem. Soc. 133*, 5329−5337.

(36) Firestone, R. A. (1994) Low-density-lipoprotein as a vehicle for targeting antitumor compounds to cancer-cells. *Bioconjugate Chem. 5*, 105−113.

(37) Zheng, G., Li, H., Yang, K., Blessington, D., Licha, K., Lund-Katz, S., Chance, B., and Glickson, J. D. (2002) Tricarbocyanine cholesteryl laurates labeled LDL: new near infrared fluorescent probes (NIRFs) for monitoring tumors and gene therapy of familial hypercholesterolemia. *Bioorg. Med. Chem. Lett. 12*, 1485−1488.
(38) Nikanjam, M., Gibbs, A. R., Hunt, C. A., Budinger, T. F., and Forte, T. M. (2007) Synthetic nano-LDL with paclitaxel oleate as a targeted drug delivery vehicle for glioblastoma multiforme. *J. Controlled Release 124*, 163−171.
(39) Zheng, G., Li, H., Zhang, M., Lund-Katz, S., Chance, B., and Glickson, J. D. (2002) Low-density lipoprotein reconstituted by pyropheophorbide cholesteryl oleate as target-specific photosensitizer. *Bioconjugate Chem. 13*, 392−396.
(40) Li, H., Zhang, Z., Blessington, D., Nelson, D. S., Zhou, R., Lund-Katz, S., Chance, B., Glickson, J. D., and Zheng, G. (2004) Carbocyanine labeled LDL for optical imaging of tumors. *Acad. Radiol. 11*, 669−677.
(41) Zheng, G., Chen, J., Li, H., and Glickson, J. D. (2005) Rerouting lipoprotein nanoparticles to selected alternate receptors for the targeted delivery of cancer diagnostic and therapeutic agents. *Proc. Natl. Acad. Sci. U. S. A. 102*, 17757−17762.
(42) Li, H., Marotta, D. E., Kim, S., Busch, T. M., Wileyto, E. P., and Zheng, G. (2005) High payload delivery of optical imaging and photodynamic therapy agents to tumors using phthalocyanine-reconstituted low-density lipoprotein nanoparticles. *J. Biomed. Opt. 10*, 41203.
(43) Wu, S. P., Lee, I., Ghoroghchian, P. P., Frail, P. R., Zheng, G., Glickson, J. D., and Therien, M. J. (2005) Near-infrared optical imaging of B16 melanoma cells via low-density lipoprotein-mediated uptake and delivery of high emission dipole strength tris-[(porphinato)zinc(II)] fluorophores. *Bioconjugate Chem. 16*, 542−550.
(44) Chen, J., Corbin, I. R., Li, H., Cao, W., Glickson, J. D., and Zheng, G. (2007) Ligand conjugated low-density lipoprotein nanoparticles for enhanced optical cancer imaging in vivo. *J. Am. Chem. Soc. 129*, 5798−5799.
(45) Corbin, I. R., and Zheng, G. (2007) Mimicking nature's nanocarrier: synthetic low-density lipoprotein-like nanoparticles for cancer-drug delivery. *Nanomedicine (Lond.) 2*, 375−380.
(46) Li, H., Gray, B. D., Corbin, I., Lebherz, C., Choi, H., Lund-Katz, S., Wilson, J. M., Glickson, J. D., and Zhou, R. (2004) MR and fluorescent imaging of low-density lipoprotein receptors. *Acad. Radiol. 11*, 1251−1259.
(47) Crich, S. G., Lanzardo, S., Alberti, D., Belfiore, S., Ciampa, A., Giovenzana, G. B., Lovazzano, C., Pagliarin, R., and Aime, S. (2007) Magnetic resonance imaging detection of tumor cells by targeting low-density lipoprotein receptors with Gd-loaded low-density lipoprotein particles. *Neoplasia 9*, 1046−1056.
(48) Geninatti-Crich, S., Alberti, D., Szabo, I., Deagostino, A., Toppino, A., Barge, A., Ballarini, F., Bortolussi, S., Bruschi, P., Protti, N., Stella, S., Altieri, S., Venturello, P., and Aime, S. (2011) MRI-guided neutron capture therapy by use of a dual gadolinium/boron agent targeted at tumour cells through upregulated low-density lipoprotein transporters. *Chem.—Eur. J. 17*, 8479−8486.